

Electrohydrodynamically Printed High-Resolution Full-Color Hybrid Perovskites

Menghua Zhu, Yongqing Duan, Nian Liu, Hegeng Li, Jinghui Li, Peipei Du, Zhifang Tan, Guangda Niu, Liang Gao,* YongAn Huang,* Zhouping Yin, and Jiang Tang*

Hybrid perovskites show enormous potential for display due to their tunable emission, high color purity, strong photoluminescence and electroluminescence. For display applications, full-color and high-resolution patterning is compulsory, however, current perovskite processing such as spin-coating fails to meet these requirements. Here, electrohydrodynamic (EHD) printing, with the unique advantages of high-resolution patterning and large scalability, is introduced to fabricate full-color perovskite patterns. Perovskite inks via simple precursor mixing are prepared to in situ crystallize tunable- and bright-photoluminescence perovskite arrays without adding antisolvent. Through optimizing the EHD printing process, a high-resolution dot matrix of 5 μm is achieved. The as-printed patterns and pictures show full color and high controllability in micrometer dimension, indicating that the EHD printing is a competitive technique for future halide perovskite-based high-quality display.

1. Introduction

Hybrid perovskites have demonstrated great performance recently, such as strong photoluminescence (PL)^[1–4] and electroluminescence (EL).^[5–10] Perovskites achieved broad tunable emission from violet to near infrared, high color purity with a full-width-at-half-maximum (FWHM) of ≈ 20 nm, and comparable external quantum efficiency over 20% to quantum dots and organic material.^[5] These indicate perovskites possess enormous potential as luminescent layers for display.^[11–16]

For the eventual application in display, full color and capability of patterning are compulsory, while high resolution is strongly preferred. To meet this requirement, the current state-of-the-art patterning strategy for perovskite is inkjet printing, which has been widely used to pattern quantum dots and

organic materials.^[17,18] This strategy is however restricted by the relative coarse resolution over 50 μm , failing to meet the requirement for high-resolution display applications.^[17–19] Besides, it is incompatible to introduce antisolvent in the printing process, which is necessary to obtain strongly luminescent perovskite film in the spin-coating process.^[20] Therefore, no full-color, strong-luminescence, and high-resolution perovskite patterns by printing have been demonstrated so far.

We chose electrohydrodynamic (EHD)^[21] printing for perovskite patterning because of its high-resolution characteristic. The EHD printing adopts electrical force to pull the jet from nozzle, rather than pushing them through a resistive

heater or piezoelectric transducer, exhibits unique advantages of high resolution (50 nm) and compatibility with wide range of inks (1–10 000 cps).^[22] During the EHD printing process, the solution on the nozzle tip is polarized by applying a high voltage potential, and this leads to an intense electric field around the pendent drop, deforming it into a cone-like shape (i.e., the Taylor cone) from whose vertex a fine jet is ejected. Previous work demonstrates the compatibility of EHD printing with a wide variety of inks, ranging from quantum dots,^[23] OLED,^[24] proteins,^[25] silver nanoparticles,^[26,27] and many others,^[28–30] and various 2D and 3D^[31–33] high-resolution structures smaller than 1 μm have been printed.

Herein we first demonstrated full-color inks for direct EHD printing, optimization of the printing parameters, and high-resolution colorful patterns and pictures. The PL wavelength could be tuned by varying the halide composite (Cl, Br, and I). By optimizing the parameters of EHD printing process, high-resolution dot arrays, as well as continuous lines and films were efficiently created. A high-resolution dot matrix of 5 μm was achieved by using a small-size nozzle. Typical microarrays exhibited bright red, green, blue, and mixing RGB PL, and complex colorful pictures such as an apple tree and a butterfly were demonstrated with precise location. We believe that the hybrid perovskites combined the EHD printing will become a new class of candidates for low-cost, full-color, and high-resolution display.

2. Results and Discussion

In order to develop directly EHD printable CsPbX₃ precursors, we first explore the preparation of CsPbX₃ inks. Generally,

Dr. M. Zhu, Dr. N. Liu, Dr. J. Li, Dr. P. Du, Dr. Z. Tan, Prof. G. Niu, Dr. L. Gao, Prof. J. Tang

Wuhan National Laboratory for Optoelectronics
Huazhong University of Science and Technology
Wuhan 430074, China

E-mail: highlight@hust.edu.cn; jtang@mail.hust.edu.cn

Dr. Y. Duan, Dr. H. Li, Prof. Y. Huang, Prof. Z. Yin
State Key Laboratory of Digital Manufacturing Equipment and
Technology

Huazhong University of Science and Technology
Wuhan 430074, China

E-mail: yahuang@hust.edu.cn

 The ORCID identification number(s) for the author(s) of this article can be found under <https://doi.org/10.1002/adfm.201903294>.

DOI: 10.1002/adfm.201903294

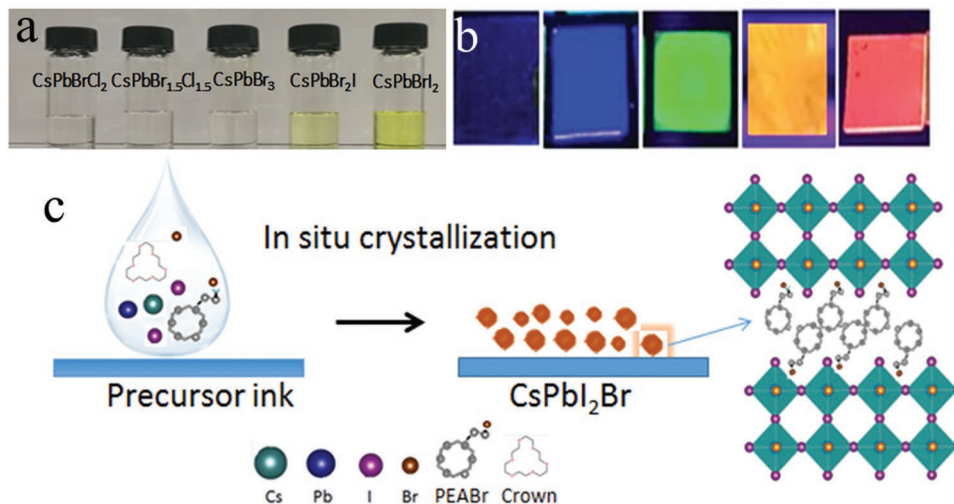


Figure 1. a) Photographs of the solution of CsPbX₃ inks. b) CsPbX₃ films with different halide compositions under a 365 nm UV lamp and c) schematic of perovskite transformation from CsPbX₃ ink to CsPbX₃ nanocrystal. The inset is the crystal structure of mixed halide perovskites.

the preparation of fluorescent perovskite film requires antisolvent to assist crystallinity or use of CsPbX₃ quantum dots. But the EHD printing process is highly incompatible with the antisolvent process, and the CsPbX₃ quantum dots also need complicated synthesis process. In this study we demonstrated an efficient and simple method to prepare single- and mixed-halide CsPbX₃ inks. The precursor inks for EHD printing were prepared by adding cesium halide (CsBr, CsCl, CsI), lead halide (PbBr₂, PbCl₂, PbI₂), 2-phenylethanamine bromide (PEABr), and a proportion of crown into dimethyl sulfoxide (DMSO) (the experimental details can be found in the Experimental Section). Here, the PEABr plays an important role in determining the film morphology, while the crown is helpful to control phase separation and the distribution of crystallite size.^[9,34] As the halide ion varies from Cl⁻ to Br⁻ and to I⁻, the color of CsPbX₃ inks changes from transparency to yellow (**Figure 1a**).

We anticipated that these inks could form in situ crystallization without antisolvent in the EHD printing process. To prove this, we fabricated the perovskite films by spin-coating precursor CsPbX₃ inks, without antisolvent, and the resulted films under UV illumination are shown in **Figure 1b**. Clearly, the PL properties can be tuned by varying the anionic composition. Similar to the bromide case, strongly luminescent CsPbX₃ films can be obtained with a clear color difference depending on halide content.^[34,35] When Cl⁻ or I⁻ was introduced into the ink, the corresponding films could emit different light under 365 nm UV excitation covering five colors of violet, blue, green, yellow, and red. Besides the tunable emission color, their photoluminescence quantum yields (PLQYs) are very high in the range of 29–80%, especially the CsPbBr₃ film shows a PLQY of > 75% (see **Table S1**, Supporting Information). The CsPbX₃ films containing Br⁻ and I⁻ exhibit relatively high PLQYs around 60%, whereas the Cl⁻ containing samples exhibit low PLQYs around 29%. A schematic in **Figure 1c** illustrates the process that the ink of CsPbX₃ transforms into CsPbX₃ nanocrystal.

To further explore the film produced via the in situ crystallization process, the measurements of scanning electron

microscopy (SEM), UV–vis absorption, X-ray diffraction (XRD), PL, and time-dependent PL were conducted. The CsPbX₃ films show smooth and uniform morphology in SEM images (**Figure S1**, Supporting Information). XRD patterns of the CsPbX₃ films are shown in **Figure 2a**, and all diffraction patterns agree well with single CsPbX₃ phase without detectable secondary phases in these mixed halide perovskites. The strong intensity and small FWHM of diffraction peaks also suggest good crystallinity of as-obtained CsPbX₃ films due to incorporating PEABr.^[36]

Figure 2b,c shows the absorption and PL spectra of the CsPbX₃ films. All CsPbX₃ films show the absorption spectra with a clear excitonic absorption peak, which proves efficiently the homogeneity of the prepared CsPbX₃ films. The typical PL peak of the CsPbBr₃ film is located at 514 nm (**Figure 2c**). The PL peak shifts to the higher (lower) energy direction as the Cl⁻ (I⁻) content increases. From the PL spectra in **Figure 2c**, it can be clearly seen that the PL peaks can be effectively tuned in the range from 446 to 630 nm by introducing Cl⁻ and I⁻ anions,^[35] covering the full spectrum for display applications. Significantly, PL peaks of CsPbX₃ films all have very small FWHM in the range of 15–29 nm, confirming high-quality emission of as-prepared CsPbX₃ films and enabling high color purity and wide-color-gamut for display applications.

Time-resolved PL measurements (**Figure 2d**) were further carried out to study the emission characteristics of these films. All PL decay curves of CsPbX₃ films can be well fitted by a biexponential equation (**Equation (1)**) and as-extracted lifetimes are summarized in **Table S2** (Supporting Information). The PL decays of CsPbX₃ films indicate radiative lifetimes in the range of 8.42–50.06 ns with faster emission from wider band-gapped CsPbX₃ films. Going from iodide to chloride via bromide the decay becomes faster, which are consistent with reported literature^[37,38]

$$A(t) = A_1 \exp\left(\frac{-t}{\tau_1}\right) + A_2 \exp\left(\frac{-t}{\tau_2}\right) \quad (1)$$

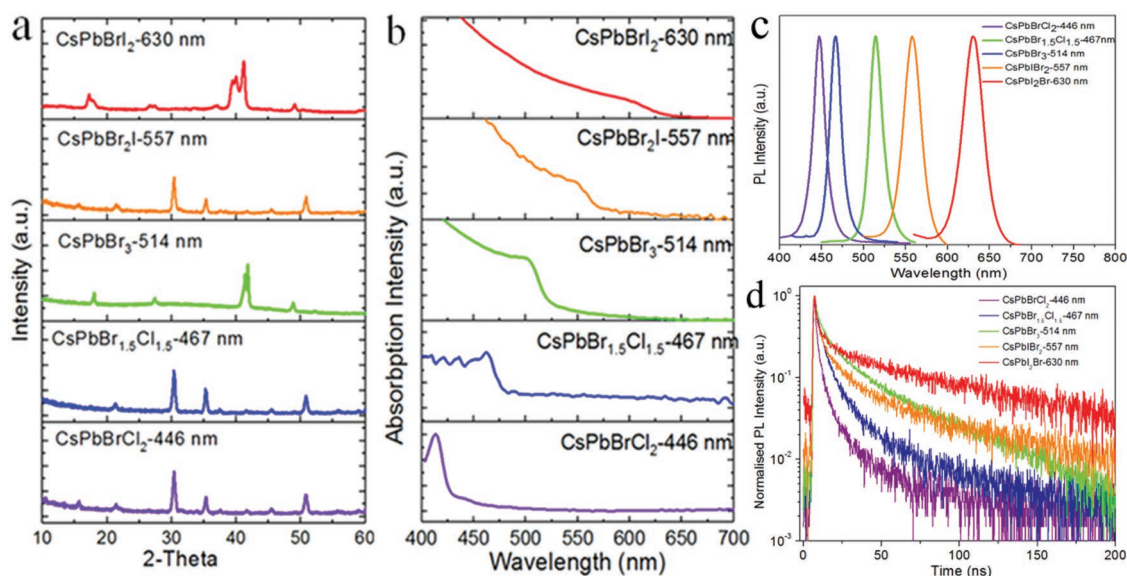


Figure 2. a) XRD patterns, b) absorption spectra, c) normalized PL spectra, and d) time-dependence PL intensity of our CsPbBrCl₂, CsPbBr_{1.5}Cl_{1.5}, CsPbBr₃, CsPbBr₂, and CsPb₂Br films prepared via in situ crystallization technique.

To place the CsPbX₃ ink at specific locations with desired size, EHD printing was employed. **Figure 3a** shows the schematic of the EHD printing setup. By attaching a high voltage between the metal-coated glass capillary and the grounded substrate, mobile ions in the ink are accumulated near the surface

at the tip of the nozzle. The Coulomb repulsion between the ions introduces a tangential stress on the liquid surface, thereby deforming the meniscus into a conical shape. The electrostatic stress is relative to the conductivity of the ink and the applied voltage. When the electrostatic stress overcomes the surface

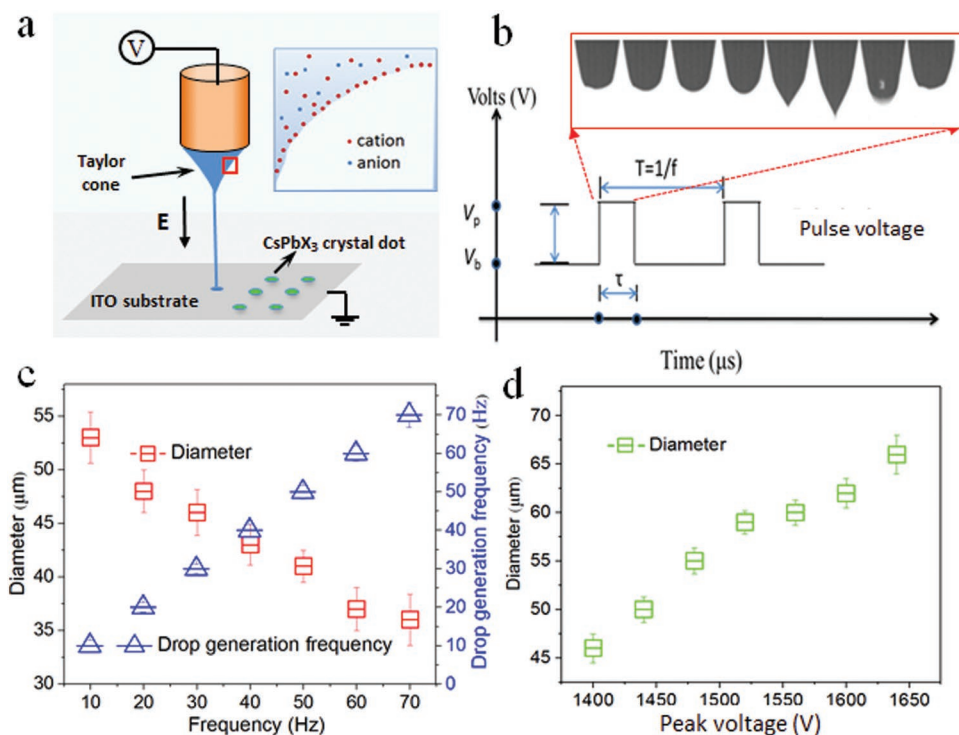


Figure 3. a) Schematic of the experimental setup for the EHD printing system. The inset shows the enlarged Taylor cone. b) Pulse voltage used in EHD printing (bottom). V_p and V_b denote the peak and baseline voltages, respectively. The image is a Taylor cone in sequence during V_p period within one cycle (upper). c) Jetting frequency and CsPbX₃ crystal dot diameter versus pulse voltage frequency. The nozzle diameter, V_p, V_b, and the duty cycle (τ/T) are fixed at 40 μm, 1100 V, 900 V, and 30%, respectively. d) The relationship between CsPbX₃ crystal dot diameter and voltage pulse peak (V_p). The nozzle diameter, V_b, f, and the duty cycle (τ/T) are fixed at 40 μm, 1000 V, 50 Hz, and 30%, respectively.

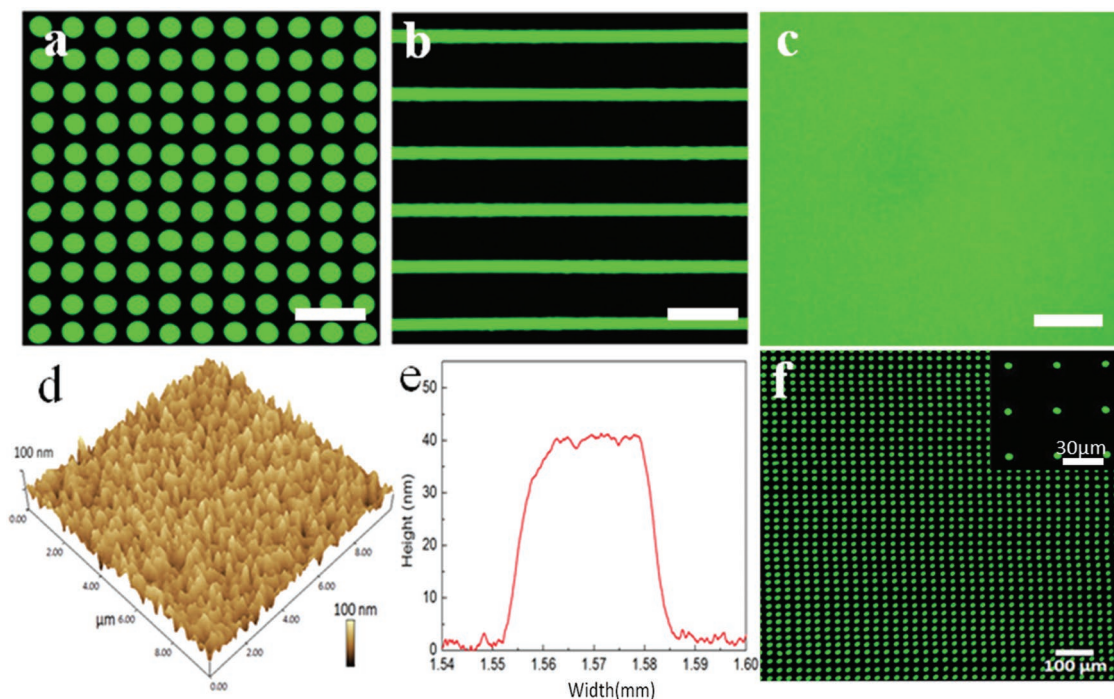


Figure 4. Typical PL images of the EHD printed a) microarrays, b) lines, and c) films composed of CsPbBr₃ dot patterns. The scale bar is 200 μm . d) AFM image and e) height profile of one single CsPbBr₃ dot. f) A high-resolution dot matrix with CsPbBr₃ dot diameter of ≈ 5 μm .

tension of the meniscus, a thin slender jet will be emitted from the apex of the Taylor cone, then the located CsPbX₃ ink will crystallize on the substrate at 40 °C.

Furthermore, to realize controllable ejection, pulses of high voltage are superimposed as shown in the bottom of Figure 3b. Voltage pulse peak (V_p) induces a jetting mode for a short duration (τ) and voltage pulse baseline (V_b) is picked slightly smaller than the critical jetting voltage to ensure that no jetting appears and the printing process is stable. The upper images in Figure 3b illustrate the changes of the ink meniscus over the jetting process, which corresponds to one drop deposited on the target substrate. Therefore, the drop generation frequency of CsPbBr₃ ink is almost equal to the pulse voltage frequency ($f = 1/T$) from the statistics of 20 drops at every frequency, as shown in Figure 3c.

The droplet size can be controlled through a combination of printing parameters including the voltage pulse and the size of the nozzle. As an example, Figure 3c,d demonstrates the dot diameter decreases with the pulse frequency and increases with the voltage pulse peak from the statistics of 20 dots. In Figure 3c, the duty cycle (τ/T) is fixed at 30%, larger pulse frequency corresponds to smaller jetting time τ , thus smaller droplet size. In Figure 3d, higher peak voltage corresponds to larger electric force applied to the ink meniscus, thus more ink is pulled down to the substrate with larger droplet size. The microphotographs of EHD printed perovskite dots with different jetting pulse frequency from 10 to 70 Hz and peak voltage from 1400 to 1640 V are shown in Figure S3 and S4 (Supporting Information).

In order to evaluate the stability of CsPbBr₃ ink during the EHD printing process, conductivity test of CsPbBr₃ ink and

the corresponding PL intensity of CsPbBr₃ dot were conducted as shown in Figure S5 (Supporting Information). The results show that the conductivity of the ink has no significant change and the PL intensity of the printed pattern experiences no degradation in brightness during intermittent printing over one month, which prove that our CsPbBr₃ ink has a good stability for EHD printing process. A stable ink is facile for the optimization of printing process, and more importantly is compulsory for the reproducible fabrication of functional patterns for future display application.

By controlling the droplet size through driving voltage and droplet position through the movement of substrate, discrete dots, continuous lines and films could be efficiently created as shown in Figure 4a–c. As mentioned above, one voltage pulse corresponds to one droplet deposited on substrate. When the distance between two droplets is small enough, the adjacent droplets will merge into lines or films. Under UV light stimulation, these CsPbBr₃ nanocomposites emit bright green light with similar brightness compared to the spin-coated film, which demonstrates that our CsPbX₃ inks are feasible for EHD printing. To evaluate the surface morphology and thickness of the patterned CsPbBr₃ microarray, Figure 4d,e shows its atomic force microscopy (AFM) image and surface height profile of a representative dot, respectively. It can be observed that this printed dot has a smooth surface with a roughness of 4 nm, and a 40 nm thickness with good conformity. The SEM image of the printed dot shown in Figure S6 (Supporting Information) also demonstrates that the surface is very smooth without pin-hole or thickness heterogeneity.

The size and PL intensity of the printed structures can be controlled by varying the printing parameters, such as the

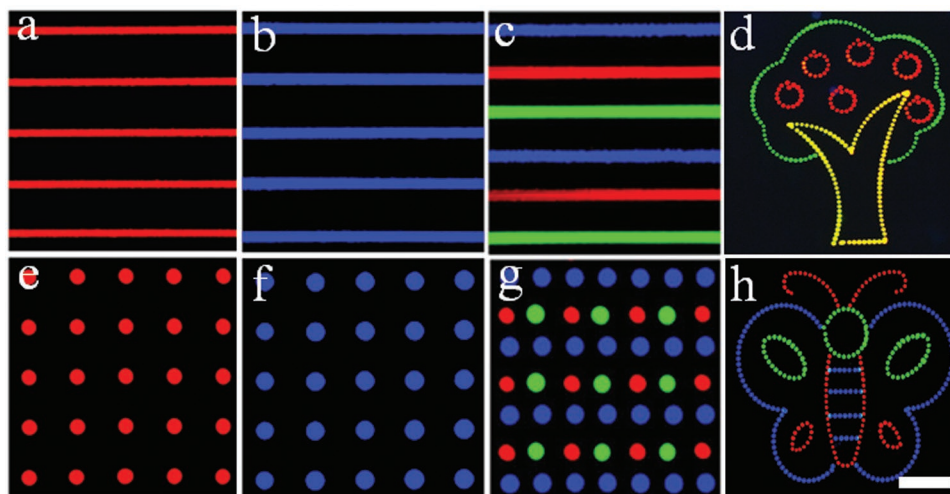


Figure 5. Typical PL images of the EHD printed microscale line arrays of a) red, b) blue, and c) RGB and dot arrays of e) red, f) blue, and g) RGB under 365 nm UV excitation. Multicolor pattern of an d) apple tree and h) a butterfly using three-color perovskite, fabricated by the method described above. All patterns and pictures use the same scale bar labeled in panel (h), which is 200 μm .

magnitude of the voltage pulse, the translation speed of the collector, the number of overprints, and so forth. To further explore the potential in reducing printed droplet size, smaller-size nozzles, such as 5 μm in diameter, were tested. By carefully optimizing the driving voltage and printing distance while using small size nozzle, EHD printing yields high-resolution arrays of perovskites with dot diameters of $\approx 5 \mu\text{m}$ as shown in Figure 4f (the nozzle diameter, printing distance, V_p , f , and the duty cycle (τ/T) are fixed at 5 μm , 10 μm , 800 V, 50 Hz, and 30%, respectively), which could match the present resolution requirement for display. This is also the key advantage of EHD printing over other printing techniques.

We further achieved blue and red perovskite microlines and microarrays using our CsPbX_3 inks and the EHD printing method, as shown in Figure 5. Figure 5a–c, e–g demonstrates fluorescent images of exactly localized red, blue and RGB microlines and microarrays. The fluorescent images of the CsPbX_3 full-color pattern under 365 nm UV excitation are homogeneous and bright. Different inks can be delivered with precise registration to different regions in the RGB arrays, as shown in Figure 5c, g. In order to further confirm the potential of EHD printing in full-color display, Figure 5d shows an apple tree precisely printed by using red, yellow and green inks, and Figure 5g displays a more complex butterfly with blue, red and green, the three primary colors. The spatially uniform patterns of fluorescence suggest their potential applications as full-color PL and EL layers. Our results demonstrate the advantages of EHD printing for high-resolution, large-scale, full-color and patterned applications, paving the way for future fabrication of full-color active matrix perovskite display.

3. Conclusions

This paper presents in situ crystallized perovskite patterns with high resolution, strong PL, and full color via EHD printing. The single- and mixed-halide CsPbX_3 inks with

full-color emission were prepared by a simple solution mixing process with the assistance of PEABr and 18-crown-6 additives. The controllable dot arrays were efficiently created with uniform PL. By adjusting the EHD printing parameters such as pulse voltage and cycle duty, in combination with the substrate movement control, various perovskite patterns such as dot and line arrays, and more complex colorful pictures are conveniently fabricated via our EHD printing technique. In addition, a high-resolution dot array smaller than 5 μm was achieved by applying small-size nozzle, which still leaves room for higher resolution. All above results demonstrated that the perovskites could combine the EHD printing to possess competitiveness for full-color, strong-luminescence, high-resolution display.

4. Experimental Section

Lead chloride (PbCl_2 , 99.9%), lead bromide (PbBr_2 , 99.9%), lead iodide (PbI_2 , 99.9%), cesium chloride (CsCl , 99.9%), cesium bromide (CsBr , 99.9%), cesium iodide (CsI , 99.9%), and DMSO were purchased from Sigma-Aldrich. PEABr (99%) was purchased from Xi'an Polymer Light Technology Corp. 18-Crown-6 was purchased from Aladdin Reagent. All reagents were used without further purification.

The perovskite inks were obtained by mixing 0.2 mmol CsBr (CsCl , CsI) and 0.2 mmol PbBr_2 (PbCl_2 , PbI_2) in DMSO with different amounts of PEABr at 80 $^\circ\text{C}$ for 2 h with constant stirring. The crown concentration in perovskite precursor was 5.0 mg mL^{-1} .^[9] Except for $\text{CsPbCl}_{1.5}\text{Br}_{1.5}$ ink (100%), the amount of PEABr in perovskite ink was 40% with a mole ratio relative to CsPbBr_3 . All the perovskite inks were filtered by 0.45 μm hydrophobic poly(tetrafluoroethylene) syringe filters before using. And all the processes were carried out in a clean room.

The perovskite ink was supplied to a glass capillary, whose diameter at the tip of 5, 20, or 40 μm was sputter-coated with gold/chromium. The ITO substrate was ultrasonically cleaned with detergent solution, acetone, deionized water, and isopropanol in sequence, and then was fixed onto a motion stage. The printing process was accomplished by applying a high voltage between the metal-coated glass capillary and the ITO substrate at a standoff height of about 10–100 μm . The applied voltage was generated by a waveform generator (33500B

Series, Keysight Technologies, Japan) and a high-voltage amplifier (MODEL 609E-6, Trek Inc., USA). During printing, the ITO substrate was heated at 40 °C to accelerate in situ crystallization. After printing, the ITO substrate with perovskite pattern was annealed at 80 °C for 1 min to complete crystallization. All printing and annealing were done in ambient conditions.

The jetting process was visualized by a high-speed camera (Dimax HD, PCO AG, Germany) with a zoom lens (magnification 1.16–13.92, Navitar Inc., USA). XRD analysis was recorded on an XRD-6000 X-ray diffractometer (Shimadzu) with Cu K α radiation ($\lambda = 1.5406 \text{ \AA}$). UV–vis spectrophotometer (PerkinElmer instruments, Lambda 950 using integrating sphere) was applied to study the optical absorption of perovskite film. PL spectra were collected using excitation of wavelength 365 nm, and the PL images of the printed microarrays were characterized by a fluorescent microscope (Nikon eclipse Ts2R). The film surface and roughness were measured by field-emission scanning electron microscopy (FE-SEM, FEI NOVA NanoSEM 450) and AFM (SPM9700), respectively.

Supporting Information

Supporting Information is available from the Wiley Online Library or from the author.

Acknowledgements

M.Z. and Y.D. contributed equally to this work. This work was financially supported by the National Natural Science Foundation of China (51761145048, 61725401, 51702107, 51605180, and 5171101030), the National Key R&D Program of China (2016YFA0700702 and 2016YFA0204000), the HUST Key Innovation Team for Interdisciplinary Promotion (2016]CTD111 and 2017KFXKJC003), the Project funded by China Postdoctoral Science Foundation (2019M652643), and the Open Foundation of Key Laboratory of Functional Inorganic Material Chemistry (Heilongjiang University), Ministry of Education (2019).

Conflict of Interest

The authors declare no conflict of interest.

Keywords

electrohydrodynamic printing, full-color displays, high-resolution patterning, perovskites

Received: April 24, 2019

Revised: June 4, 2019

Published online:

- [1] I. L. Braly, D. W. Qilettes, L. M. Pazos-Outon, S. Burke, M. E. Ziffer, D. S. Ginger, H. W. Hillhouse, *Nat. Photonics* **2018**, *12*, 355.
- [2] C. Bi, S. Wang, W. Wen, J. Yuan, G. Cao, J. Tian, *J. Phys. Chem. C* **2018**, *122*, 5151.
- [3] D. M. Kroupa, J. Y. Roh, T. J. Milstein, S. E. Creutz, D. R. Gamelin, *ACS Energy Lett.* **2018**, *3*, 2390.
- [4] N. Mondal, A. De, A. Samanta, *ACS Energy Lett.* **2019**, *4*, 32.
- [5] K. Lin, J. Xing, L. N. Quan, F. P. G. Arquer, X. Gong, J. Lu, L. Xie, W. Zhao, D. Zhang, C. Yan, W. Li, X. Liu, Y. Lu, J. Kirman, E. H. Sargent, Q. Xiong, Z. Wei, *Nature* **2018**, *562*, 245.
- [6] Z. Li, Z. Chen, Y. Yang, Q. Xue, H.-L. Yip, Y. Cao, *Nat. Commun.* **2019**, *10*, 1027.
- [7] Y. Gao, C. Huang, C. Hao, S. Sun, L. Zhang, C. Zhang, Z. Duan, K. Wang, Z. Jin, N. Zhang, A. V. Kildishev, C.-W. Qiu, Q. Song, S. Xiao, *ACS Nano* **2018**, *12*, 8847.
- [8] J. Mao, H. Lin, F. Ye, M. Qin, J. M. Burkhartsmeyer, H. Zhang, X. Lu, K. S. Wong, W. C. H. Choy, *ACS Nano* **2018**, *12*, 10486.
- [9] M. Ban, Y. Zou, J. P. H. Rivett, Y. Yang, T. H. Thomas, Y. Tan, T. Song, X. Gao, D. Credgington, F. Deschler, H. Sirringhaus, B. Sun, *Nat. Commun.* **2018**, *9*, 3892.
- [10] Y. Cao, N. Wang, H. Tian, J. Guo, Y. Wei, H. Chen, Y. Miao, W. Zou, K. Pan, Y. He, H. Cao, Y. Ke, M. Xu, Y. Wang, M. Yang, K. Du, Z. Fu, D. Kong, D. Dai, Y. Jin, G. Li, H. Li, Q. Peng, J. Wang, W. Huang, *Nature* **2018**, *562*, 249.
- [11] M. Liu, G. Zhong, Y. Yin, J. Miao, K. Li, C. Wang, X. Xu, C. Shen, H. Meng, *Adv. Sci.* **2017**, *4*, 1700335.
- [12] A. Pan, M. J. Jurow, F. Qiu, J. Yang, B. Ren, J. J. Urban, L. He, Y. Liu, *Nano Lett.* **2017**, *17*, 6759.
- [13] J. Sun, F. T. Rabouw, X. Yang, X. Huang, X. Jing, S. Ye, Q. Y. Zhang, *Adv. Funct. Mater.* **2017**, *27*, 1704371.
- [14] Y. Liu, Q. Xu, S. Chang, Z. Lv, S. Huang, F. Jiang, X. Zhang, G. Yang, X. Tong, S. Hao, Y. Ren, *Phys. Chem. Chem. Phys.* **2018**, *20*, 19950.
- [15] D. Yu, F. Cao, Y. Gao, Y. Xiong, H. Zeng, *Adv. Funct. Mater.* **2018**, *28*, 1704537.
- [16] Z. Zhao, Z. Wu, J. Cheng, L. Jing, Y. Hou, *J. Phys. Chem. C* **2018**, *122*, 16887.
- [17] Y. Liu, F. Li, L. Qiu, K. Yang, Q. Li, X. Zheng, H. Hu, T. Guo, C. Wu, T. W. Kim, *ACS Nano* **2019**, *13*, 2042.
- [18] M. Zhu, W. Liu, W. Ke, L. Xie, P. Dong, F. Hao, *ACS Appl. Mater. Interfaces* **2019**, *11*, 666.
- [19] C. H. Lin, Q. Zeng, E. Lafalce, S. Yu, M. J. Smith, Y. J. Yoon, Y. Chang, Y. Jiang, Z. Lin, Z. V. Vardeny, V. V. Tsukruk, *Adv. Opt. Mater.* **2018**, *6*, 1801245.
- [20] Z. Zhang, J. Yao, L. Liang, X. Tong, Y. Lin, F. Liang, H. Yao, L. Luo, *ACS Appl. Mater. Interfaces* **2018**, *10*, 39441.
- [21] J. U. Park, M. Hardy, S. J. Kang, K. Barton, K. Adair, D. K. Mukhopadhyay, C. Y. Lee, M. S. Strano, A. G. Alleyne, J. G. Georgiadis, P. M. Ferreira, J. A. Rogers, *Nat. Mater.* **2007**, *6*, 782.
- [22] M. S. Onses, E. Sutanto, P. M. Ferreira, A. G. Alleyne, J. A. Rogers, *Small* **2015**, *11*, 4237.
- [23] B. H. Kim, M. S. Onses, J. B. Lim, S. Nam, N. Oh, H. Kim, K. J. Yu, J. W. Lee, J.-H. Kim, S.-K. Kang, C. H. Lee, J. H. Kim, N. H. Kim, C. Leal, M. Shim, J. A. Rogers, *Nano Lett.* **2015**, *15*, 969.
- [24] K. Kim, G. Kim, B. R. Lee, S. Ji, S. Y. Kim, B. W. An, M. H. Song, J. U. Park, *Nanoscale* **2015**, *7*, 13410.
- [25] K. Shigetani, Y. He, E. Sutanto, S. Kang, A. P. Le, R. G. Nuzzo, A. G. Alleyne, P. M. Ferreira, Y. Lu, J. A. Rogers, *J. Am. Chem. Soc.* **2012**, *84*, 10012.
- [26] X. Wang, L. Xu, G. Zheng, W. Cheng, D. J. Sun, *Sci. China: Technol. Sci.* **2012**, *55*, 1603.
- [27] K. Wang, M. D. Paine, J. P. Stark, *J. Appl. Phys.* **2009**, *106*, 024907.
- [28] Y. Ding, Y. Duan, Y. Huang, *Energy Technol.* **2015**, *3*, 351.
- [29] S. Coppola, G. Nasti, V. Vespieni, S. Grilli, P. Russo, P. J. Ferraro, *J. Micro Nanolithogr. MEMS MOEMS* **2018**, *17*, 031206.
- [30] W. Zou, H. Yu, P. Zhou, L. Liu, *Mater. Des.* **2019**, *166*, 274158.
- [31] B. W. An, K. Kim, H. Lee, S. Y. Kim, Y. Shim, D. Y. Lee, J. Y. Song, J. U. J. Park, *Adv. Mater.* **2015**, *27*, 4322.
- [32] H. T. Yudistira, A. P. Tenggara, S. S. Oh, N. VuDat, M. Choi, C. G. Choi, D. Byun, *J. Micromech. Microeng.* **2015**, *25*, 045006.
- [33] K. Li, D. Wang, Q. Wang, K. Song, J. Liang, Y. Sun, M. Madoua, *Macromol. Mater. Eng.* **2018**, *303*, 1800345.

- [34] A. Dutta, R. K. Behera, P. Pal, S. Baitalik, N. Pradhan, *Angew. Chem.* **2019**, *131*, 5608.
- [35] J. Song, J. Li, X. Li, L. Xu, Y. Dong, H. Zeng, *Adv. Mater.* **2015**, *27*, 7162023.
- [36] D. Zhang, L. Gu, Q. Zhang, Y. Lin, D. Lien, M. Kam, S. Poddar, E. C. Garnett, A. Javey, Z. Fan, *Nano Lett.* **2019**, *21*, 253.
- [37] Y. Tong, E. P. Yao, A. Manzi, E. Bladt, K. Wang, M. Doeblinger, S. Bals, P. Mueller-Buschbaum, A. S. Urban, L. Polavarapu, J. Feldmann, *Adv. Mater.* **2018**, *30*, 1801117.
- [38] L. Protesescu, S. Yakunin, M. I. Bodnarchuk, F. Krieg, R. Caputo, C. H. Hendon, R. X. Yang, A. Walsh, M. V. Kovalenko, *Nano Lett.* **2015**, *15*, 3692.